

Stability of Discrete-Time Bilateral Teleoperation Control

M. Tavakoli, A. Aziminejad, R.V. Patel, M. Moallem

Department of Electrical & Computer Engineering, University of Western Ontario, London, ON, Canada N6A 5B9
Canadian Surgical Technologies & Advanced Robotics (CSTAR), 339 Windermere Road, London, ON, Canada N6A 5A5

Abstract—Discretization of a stabilizing continuous-time bilateral teleoperation controller for digital implementation may not necessarily lead to stable teleoperation. This paper addresses the stability of master-slave teleoperation under discrete-time bilateral control. Stability regions are determined in the form of conditions involving the sampling period, control gains including the damping introduced by the controller, and environment stiffness. Due to the tradeoff between stability and transparency in bilateral teleoperation, such stability boundaries are of particular importance when the teleoperation system has good transparency.

I. Introduction

Problems with haptic teleoperation stability arise when a bilateral controller designed in the continuous-time (CT) domain is converted into the discrete-time (DT) domain for implementation as a digital controller. Due to the wealth of CT design methods, discretizing predesigned CT controllers rather than direct DT design is very common and, in teleoperation control, overwhelmingly the method of choice.

Since a zero-order hold (ZOH) creates energy leaks that can make an otherwise passive system non-passive [1], some researchers have studied the effect of sampled-data control on system passivity [2], [3] or stability [4]. For the problem of haptic rendering of a discretely-simulated virtual wall, Colgate and Schenkel [5] found the necessary and sufficient conditions for passivity of the virtual wall as

$$b > \frac{k_w T}{2} + b_w \quad (1)$$

where $b > 0$ is the haptic interface damping and $k_w > 0$ and $b_w > 0$ are the virtual wall stiffness and damping, respectively. It is confirmed by (1) that passivity competes with transparency, which requires high k_w and b_w . Abbott et al. [6] found an upper bound on virtual wall stiffness as a function of sampling rate, encoder resolution and friction in order to ensure virtual wall passivity. Also, Gil et al. [7] applied the Routh-Hurwitz criterion to the characteristic equation of the system to obtain a necessary and sufficient condition for stability that can be approximated by

$$b > \frac{k_w T}{2} - b_w. \quad (2)$$

Therefore, the stability condition (2) is less conservative than the passivity condition (1) and allows for higher transparency [8]. Moreover, the haptic interface damping b and the virtual wall damping b_w both help to achieve stability with longer sampling periods and for stiffer environments.

While research so far has focused on the passivity or stability of haptic interaction with a discretely-simulated virtual wall, this paper addresses the stability of master-slave teleoperation under discrete-time bilateral control. In this paper, we consider constant sampling periods and the 4-channel bilateral teleoperation architecture [9], which can represent other teleoperation methods including position-error based (PEB) and direct force reflection (DFR) control through appropriate selection of its control gains. Regions of

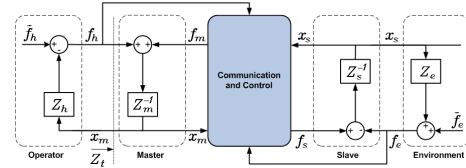


Fig. 1. Block diagram of a master-slave teleoperation system.

stability of the discrete-time controlled teleoperation system are obtained in the form of conditions on the sampling period, environment stiffness and control parameters.

II. Teleoperation Stability Analysis Tools

The block diagram of a bilateral master-slave system is shown in Figure 1. Here, $\hat{f}_h(t)$ and $\hat{f}_e(t)$ are respectively the operator's and the environment's exogenous input forces and are independent of the teleoperation system behavior. The hand/master and the slave/environment interactions (force or torque) are denoted by $f_h(t)$ and $f_e(t)$, respectively. The master and the slave positions and control signals (force or torque) are shown by $x_m(t)$, $x_s(t)$, $f_m(t)$ and $f_s(t)$, respectively. The impedances $Z_h(s)$, $Z_e(s)$, $Z_m(s)$ and $Z_s(s)$ denote the dynamic characteristics of the human operator's hand, the remote environment, the master robot, and the slave robot, respectively. The impedance $Z_t(s)$ is the perception of the user about the environment impedance $Z_e(s)$. Based on Figure 1, the dynamics of the master and the slave can be written in the frequency domain as:

$$\begin{aligned} F_m + F_h &= Z_m X_m = M_m s^2 X_m \\ F_s - F_e &= Z_s X_s = M_s s^2 X_s \end{aligned} \quad (3)$$

where M_m and M_s are the master and the slave inertias, respectively. The teleoperation system of Figure 1 can be modeled as a two-port network with the following hybrid matrix representation

$$\begin{bmatrix} F_h \\ -X_s \end{bmatrix} = \begin{bmatrix} h_{11}(s) & h_{12}(s) \\ h_{21}(s) & h_{22}(s) \end{bmatrix} \begin{bmatrix} X_m \\ F_e \end{bmatrix} \quad (4)$$

For analysis of stability of a teleoperation system, the knowledge of the human operator and the environment dynamics are needed in addition to the teleoperation system model (4). Analysis of passivity, however, is independent of $Z_h(s)$ and $Z_e(s)$, and only assumes that the environment is passive ($\tilde{f}_e = 0$) and the operator is passive in the sense that he/she does not perform actions that will make the teleoperation system unstable. With passive but otherwise arbitrary terminations $Z_h(s)$ and $Z_e(s)$ and using Llewellyn's criterion or based on the singular values of the scattering matrix of the teleoperation system, stability conditions independent of the human operator and the environment (*absolute stability*) may be derived. The scattering matrix $S(s)$ of a teleoperation system satisfies $F - X = S(s)(F + X)$ where $F = [F_h \ F_e]^T$ and $X = [X_m \ -X_s]^T$.

Analysis of stability based on Llewellyn's criterion or singular values of the scattering matrix is conservative as

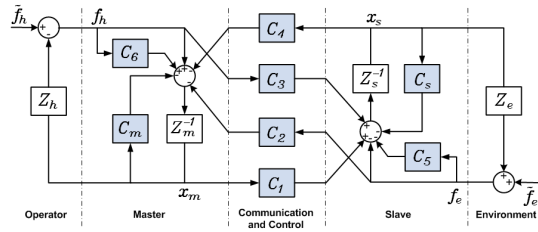


Fig. 2. The 4-channel bilateral teleoperation system. The shaded blocks represent control components.

it ensures stability regardless of the teleoperation system's terminations (i.e., the human operator and the remote environment). While it is useful to remove any assumption on the operator, the environment model can be incorporated into the analysis for less conservative stability regions. With the remote environment impedance Z_e , i.e., $F_e = Z_e X_s$, the general teleoperation system given by (4) has the following transfer function from F_h to X_m :

$$\frac{X_m}{F_h} = \frac{1 + h_{22}Z_e}{h_{11}(1 + h_{22}Z_e) - h_{12}h_{21}Z_e} \quad (5)$$

Assuming the environment is modeled by a linear spring, $Z_e = k_e$, the characteristic equation for the transfer function from F_h to X_m (and to any other output) is given by

$$h_{11}s + k_e(h_{11}h_{22} - h_{12}h_{21}) = 0 \quad (6)$$

The characteristic equation (6) must have no zeros in the right-half plane (RHP) for the teleoperation system to be stable regardless of the operator dynamics.

To remove any assumption on the human operator's impedance Z_h , we model the operator as an exogenous input force. In practice, the human operator with a finite impedance dynamic range acts as a negative feedback and only improves the stability [10], so the stability regions found in this paper correspond to a *worst-case* scenario and are independent of the operator's dynamical characteristics. Also, note that we have assumed linear models in (3) and have neglected nonlinear terms such as friction and encoder quantization. It is well known that friction plays a stabilizing role in a teleoperation system. Indeed, it has been shown that Coulomb friction can dissipate the energy introduced by encoder quantization [11], [6]. Therefore, stability analysis using linear models results in worst-case stability conditions [12].

III. Continuous-Time Bilateral Teleoperation Stability

Figure 2 depicts a 4-channel (4CH) bilateral teleoperation architecture [9]. The compensators C_5 and C_6 in Figure 2 constitute local force feedback at the slave side and the master side, respectively. Selecting $C_1 = C_s$, $C_4 = -C_m$ and $C_2 = C_3 = C_5 = C_6 = 0$ amounts to position-error based (PEB) control and $C_1 = C_s$, $C_2 = 1$ and $C_3 = C_4 = C_5 = C_6 = C_m = 0$ leads to direct force reflection (DFR) control.

The controllers C_m and C_s are usually chosen as proportional-derivative controllers. Taking $C_m = k_{v_m}s + k_{p_m}$ and $C_s = k_{v_s}s + k_{p_s}$, as shown in [13], the PEB teleoperation architecture is absolutely stable if $k_{v_m}, k_{p_m}, k_{v_s}, k_{p_s} > 0$ and

$$\frac{C_m(s)}{C_s(s)} = \alpha \quad (7)$$

where α is a nonnegative constant. Throughout this paper, we assume (7) in the general case of 4-channel control. With direct force reflection teleoperation, $\alpha = 0$.

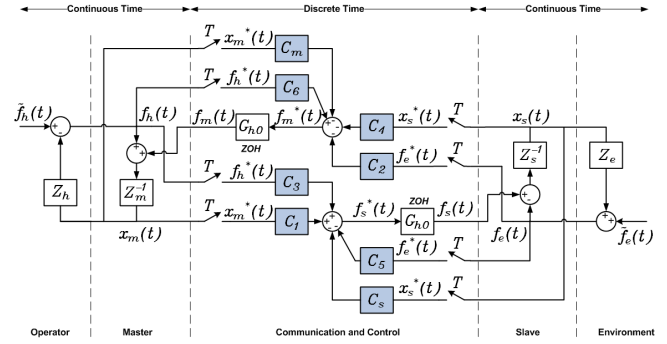


Fig. 3. A digitally-controlled 4-channel bilateral teleoperation system.

For ideal transparency, i.e., $x_m = x_s$ and $f_h = f_e$ regardless of the operator and environment dynamics, the hybrid matrix in (4) should be

$$H = \begin{bmatrix} 0 & 1 \\ -1 & 0 \end{bmatrix} \quad (8)$$

which happens in the 4CH system for

$$C_1 = Z_{ts}, \quad C_2 = 1 + C_6, \quad C_3 = 1 + C_5, \quad C_4 = -Z_{tm} \quad (9)$$

By selecting the bilateral teleoperation controllers as in (9), the hybrid and scattering matrices of the 4CH teleoperation system become

$$H = \begin{bmatrix} 0 & D \\ -D & 0 \end{bmatrix}, \quad S = \begin{bmatrix} \frac{-D^2 + D^2}{2D^2} & \frac{2D^2}{2D^2} \\ \frac{2D^2}{2D^2} & \frac{D^2 - D^2}{2D^2} \end{bmatrix} \quad (10)$$

where $D = -C_3C_4 + Z_{ts}(1 + C_6)$, $Z_{tm} = Z_m + C_m$ and $Z_{ts} = Z_s + C_s$. Using either Llewellyn's criterion or the scattering matrix condition, the ideally transparent teleoperation system is stable iff D is RHP-analytic. If so, H simplifies to (8), and S is reduced to an off-diagonal, reciprocal matrix with both of its singular values equal to 1. Since under ideal transparency condition the system is reciprocal, the stability of the system can be deduced¹.

As a result, under ideal transparent conditions, the teleoperation system stability critically depends on exact implementation of control laws because any departure from (9) risks violating $\bar{\sigma} \leq 1$. Such a low stability margin for the ideally transparent teleoperator can be explained by the trade-off that exists between stability and transparency in bilateral teleoperation [9]. Therefore, it is important to investigate the effect of discrete-time control law implementation on the teleoperation system stability. It must be noted that while this research has been mainly motivated by the critical stability of an ideally transparent 4CH teleoperation system, in the stability analysis that follows we make no assumptions on C_2 , C_3 , C_5 or C_6 as was done in (9), in order to cover all teleoperation methods including PEB and DFR architectures.

IV. Discrete-Time Bilateral Teleoperation Modeling

The 4-channel architecture of Figure 2 under discrete-time control is shown in Figure 3. As shown, the operator, the master, the slave and the environment remain continuous-time entities. For an input $f(t)$ to an ideal sampler starting at $t = 0$, the output is $f^*(t) = \sum_{k=0}^{\infty} f(kT)\delta(t - kT)$ where T is the sampling period. Since $z = e^{sT}$, the Laplace and Z

¹The necessary and sufficient condition for absolute stability of a reciprocal two-port network ($S_{12} = S_{21}$) with an RHP-analytic scattering matrix $S(s)$ is $\bar{\sigma}[S(j\omega)] \leq 1$ where $\bar{\sigma}$ represents the maximum singular value of $S(j\omega)$.

transforms of the sampled-data signal $f^*(t)$ are $F^*(s) = \mathcal{L}[f^*(t)] = \sum_{k=0}^{\infty} f(kT)e^{-kTs}$ and $F(z) = \mathcal{Z}[f^*(t)] = F^*(s)|_{s=\frac{1}{T}\ln z}$. In Figure 3, the two zero-order hold (ZOH) blocks reconstruct continuous-time control signals $f_m(t)$ and $f_s(t)$ from discrete-time counterparts $f_m^*(t)$ and $f_s^*(t)$ via the following transfer function:

$$G_{h0}(s) = \frac{1 - e^{-Ts}}{s} \quad (11)$$

With the 4-channel structure shown in Figure 3, since $C_m, C_s, C_1, \dots, C_6$ are all discrete-time controllers, the discrete-time control signals for the master and the slave can be written as

$$\begin{aligned} F_m^* &= -C_m X_m^* - C_4 X_s^* + C_6 F_h^* - C_2 F_e^* \\ F_s^* &= C_1 X_m^* - C_s X_s^* + C_3 F_h^* - C_5 F_e^* \end{aligned} \quad (12)$$

Using (12) and substituting for $F_m = G_{h0}F_m^*$ and $F_s = G_{h0}F_s^*$ in (3), the closed-loop dynamics of the master and the slave in discrete-time are written as

$$\begin{aligned} X_m(z) &= \mathcal{Z}[Z_m^{-1}F_h] + \mathcal{Z}[Z_m^{-1}G_{h0}](-C_m(z)X_m(z) \\ &\quad - C_4(z)X_s(z) + C_6(z)F_h(z) - C_2(z)F_e(z)) \\ X_s(z) &= -\mathcal{Z}[Z_s^{-1}F_e] + \mathcal{Z}[Z_s^{-1}G_{h0}](C_1(z)X_m(z) \\ &\quad - C_s(z)X_s(z) + C_3(z)F_h(z) - C_5(z)F_e(z)) \end{aligned} \quad (13)$$

With $Z_m = M_m s^2$ and $Z_s = M_s s^2$, we have

$$\mathcal{Z}[Z_{m,s}^{-1}G_{h0}] = \frac{T^2}{2M_{m,s}} \frac{z+1}{(z-1)^2} \quad (14)$$

where, for brevity, commas in subscripts mean ‘‘or’’ and present multiple equations. Using Tustin’s method, the PD controller C_s is discretized as $C_s = k_{vs} \frac{2(z-1)}{T(z+1)} + k_{ps}$ and C_m is obtained from (7). Also, $C_1 = C_s$ and $C_4 = -C_m$ are selected, which involve a slight departure from the ideal transparent design (9) as the acceleration terms are neglected to reduce noise. At this stage, we make no assumptions on C_2, C_3, C_5 or C_6 in order to cover all teleoperation methods.

Note that in (13), $\mathcal{Z}[Z_m^{-1}F_h] \neq Z_m^{-1}(z)F_h(z)$ and $\mathcal{Z}[Z_s^{-1}F_e] \neq Z_s^{-1}(z)F_e(z)$ because the master and the slave transfer functions Z_m^{-1} and Z_s^{-1} operate in continuous time (i.e., F_h and F_e are not sampled). To be able to derive a hybrid model representation from (13), we need to approximate $\mathcal{Z}[Z_m^{-1}F_h]$ and $\mathcal{Z}[Z_s^{-1}F_e]$ by products of $F_h(z)$ and $F_e(z)$ given that Z_m^{-1} and Z_s^{-1} are double integrators.

Two Taylor series expansions of $g(t) = \int_0^t \int_0^s f(r)drds$ around the sampling instant kT are

$$\begin{aligned} g(kT \pm T) &= g(kT) \pm Tg'(kT) + (T^2/2)g''(kT) \\ &\quad \pm (T^3/6)g'''(kT) + \mathcal{O}(T^4) \end{aligned} \quad (15)$$

Since $g''(kT) = f(kT)$, summing $g(kT+T)$ and $g(kT-T)$ and taking \mathcal{Z} transform on both sides gives the Verlet double integrator

$$G(z) = T^2 \frac{z}{(z-1)^2} F(z) = V_3(z)F(z) \quad (16)$$

which is an order more accurate than integration by the Euler method as third-order terms in the Taylor expansions cancel out. The double integration precision can be increased to $\mathcal{O}(T^6)$ where fifth-order terms cancel out:

$$G(z) = \frac{4T^2}{3} \frac{z(z^2+z+1)}{(z^2-1)^2} F(z) = V_5(z)F(z) \quad (17)$$

where the Tustin’s transformation $\frac{2(z-1)}{T(z+1)}$ has replaced the derivative operator s .

Based on (16) and (17),

$$\mathcal{Z}[Z_{m,s}^{-1}F_{h,e}] = \frac{V_i(z)}{M_{m,s}} F_{h,e}(z), \quad i = 3, 5 \quad (18)$$

Replacing (14) and (18) in (13) gives the hybrid model of the digitally-controlled teleoperation system as

$$\begin{bmatrix} F_h(z) \\ -X_s(z) \end{bmatrix} = \begin{bmatrix} h_{11}(z) & h_{12}(z) \\ h_{21}(z) & h_{22}(z) \end{bmatrix} \begin{bmatrix} X_m(z) \\ F_e(z) \end{bmatrix} \quad (19)$$

V. Discrete-Time Bilateral Teleoperation Stability

Using the discrete-time hybrid parameters (19) in (6), the characteristic equation of the teleoperation system is obtained. The characteristic equation has 10 roots on the unit circle irrespective of the system parameters, leaving for stability analysis a fourth- and an eight-order polynomial in z when $i = 3$ and $i = 5$ in (18), respectively. To be able to apply the Routh-Hurwitz criterion to the simplified characteristic equation, we consider the r -transformation $z = (r+1)/(r-1)$ which maps the interior of the unit circle $|z| = 1$ onto the left half of the r -plane. The result is a fourth-order polynomial in r if $i = 3$ and a sixth-order polynomial in r (after factoring out r^2) if $i = 5$. To derive the stability requirements based on these characteristic equations, we frequently utilize the following basic facts.

- The polynomial $r^n + b_1 r^{n-1} + \dots + b_n = 0$ is Hurwitz (i.e., its coefficients are positive real numbers and its zeros are located in the left half-plane of the complex plane) if and only if for $j = 1, \dots, n$,

$$\Delta_j = \begin{vmatrix} b_1 & 1 & 0 & \dots & 0 \\ \vdots & \vdots & \vdots & \ddots & \vdots \\ b_{2j-1} & b_{2j-2} & b_{2j-3} & \dots & b_{2j} \end{vmatrix} > 0 \quad (20)$$

- The quadratic equation $ax^2 + bx + c = 0$ has two solutions x_1 and x_2 for which $x_1 + x_2 = -b/a$ and $x_1 x_2 = c/a$. If $b^2 - 4ac < 0$ (two complex conjugate roots), the expression $ax^2 + bx + c$ has the same sign as a regardless of x . If $b^2 - 4ac \geq 0$ (two real roots), $ax^2 + bx + c$ has the same sign as a only for $x < \min\{x_1, x_2\}$ or $x > \max\{x_1, x_2\}$. Moreover, the two real roots will have the same sign if $c/a > 0$ (positive if $b/a < 0$, negative if $b/a > 0$).

Each Δ_j is a function of $T, k_e, C_2, C_5, C_s, \alpha, Z_m$ and Z_s but not a function of C_3 or C_6 as the last two parameters only appear in the numerator of (5). Therefore, conditions (20) determine the space of stabilizing controllers, sampling time, and environment stiffness for given master and slave inertias. In addition, for practical reasons, we impose the following conditions on the control parameters C_2 and C_5 :

- The force feedback gain C_2 should be nonnegative, otherwise the direction of the reflected force will be wrong.

$$C_2 \geq 0 \quad (21)$$

- The slave local feedback gain C_5 should be nonpositive as a measure to counteract the environment force f_e but it should not be less than -1 (note the term $-(1+C_5)f_e$ in the control effort of the slave in Figures 2 and 3.)

$$-1 \leq C_5 \leq 0 \quad (22)$$

Each Δ_j is a polynomial of order $j-1$ in k_e . Therefore, for given master and slave inertias and to have stable

teleoperation, conditions (20) set lower and upper bounds on the environment stiffness as

$$\gamma_1 \leq k_e \leq \gamma_2 \quad (23)$$

where γ_1 and γ_2 are functions of the control gains and the sampling time. With regard to (23), two points should be considered:

- It is desirable to have

$$\gamma_2 \rightarrow +\infty, \quad (24)$$

in order to have maximum stability robustness against variations in k_e .

- It is imperative to have

$$\gamma_1 = 0, \quad (25)$$

otherwise the teleoperation system would not be stable when the slave is in free space.

It turns out that $i = 3$ and $i = 5$ in (18), which correspond to $n = 4$ and $n = 6$ in (20) respectively, lead to an almost identical lower bound γ_1 , thus we proceed with $i = 3$ for less complexity. Each Δ_j has a factor $k_{p_s}^j [C_2 + \alpha(1 + C_5)]^j$ in its denominator. Therefore, knowing that $k_{p_s} > 0$, we must have

$$C_2 + \alpha(1 + C_5) > 0 \quad (26)$$

in order to prevent abrupt sign changes in Δ_j , $j = 1, \dots, 4$. Otherwise, an infinitesimal change in C_2 or C_5 such that $C_2 + \alpha(1 + C_5)$ crosses zero causes the terms of odd order (Δ_1 and Δ_3) to change sign and destabilizes the system. Fortunately, (26) is ensured due to constraints (21) and (22) that we have already assumed for C_2 and C_5 .

In the rest of this Section, we derive additional conditions for having $\Delta_j > 0$ for each j . Without loss of generality, since we are only concerned about conditions for stability, we assume strict inequalities. Replacing inequalities by equalities in the the stability conditions that will follow gives the borderline of stability and instability.

A. $j = 1$

The expression for Δ_1 is independent of k_e and $\Delta_1 > 0$ imposes the following lower bound on k_{v_s}

$$k_{v_s} > \varphi_1(T, k_{p_s}, C_i, \alpha) = k_{p_s} T \left(1 - \frac{\alpha/2}{C_2 + \alpha(1 + C_5)} \right) \quad (27)$$

or, alternatively, the following upper bound on T

$$T < \zeta_1(k_{v_s}, k_{p_s}, C_i, \alpha) = \frac{k_{v_s}}{k_{p_s} \left(1 - \frac{\alpha/2}{C_2 + \alpha(1 + C_5)} \right)} \quad (28)$$

B. $j = 2$

The expression for Δ_2 involves k_e^{-1} ,

$$\Delta_2 = Q_2(M_2 + N_2/k_e) \quad (29)$$

where M_2 and N_2 are functions of the control and system parameters and the sampling time, and Q_2 is a positive term. Assuming $T^2, T^3 \approx 0$ for mathematical simplicity, the solution to $\Delta_2 = 0$ is

$$k_{e_0} = \frac{-N_2}{M_2} = \frac{T k_{p_s}^2 (M_m + \alpha M_s)(C_2 + \alpha C_5)}{m_2 k_{v_s}^2 + n_2 k_{v_s} + p_2} \quad (30)$$

where

$$\begin{aligned} m_2 &= -2T[C_2 + \alpha(1 + C_5)][C_2 + \alpha(C_5 + 1/2)] \\ n_2 &= 2M_m(1 + C_5)[C_2 + \alpha(1 + C_5)] \\ p_2 &= -TM_m k_{p_s} [(1 + C_5)(C_2 + \alpha(1 + C_5)) + C_2] \end{aligned}$$

Due to (21), (22) and (26), we have $n_2 > 0$ and $p_2 < 0$. Also, as will be seen later for that case that $j = 3$, $\Delta_3 > 0$ requires that

$$C_2 + \alpha C_5 < 0 \quad (31)$$

implying that $N_2 > 0$.

In order to ensure (25), it is necessary that $k_{e_0} < 0$ (because if Δ_2 changes sign at a positive k_e , then (25) would be violated). To this end, since $N_2 > 0$, M_2 needs to be positive. To find the conditions under which $M_2 > 0$, we distinguish the following four cases:

- Case 1: $m_2 < 0$ and $n_2^2 - 4m_2 p_2 < 0$. The quadratic polynomial M_2 will never be positive for any k_{v_s} , and therefore this case is not of interest.
- Case 2: $m_2 < 0$ and $n_2^2 - 4m_2 p_2 \geq 0$. Since $n_2 > 0$ and $p_2 < 0$, $M_2 = 0$ has two real positive solutions implying that $M_2 > 0$ holds only if k_{v_s} is between these two solutions.
- Case 3: $m_2 > 0$ and $n_2^2 - 4m_2 p_2 < 0$. This is impossible because we know $p_2 < 0$.
- Case 4: $m_2 > 0$ and $n_2^2 - 4m_2 p_2 \geq 0$. Since $n_2 > 0$ and $p_2 < 0$, $M_2 = 0$ has one real positive and one real negative solution and $M_2 > 0$ holds if k_{v_s} (positive) is greater than the positive root.

Similar to a discretely-simulated virtual wall (conditions (1) and (2)), Case 2 is not opted for as an upper bound on k_{v_s} is not desirable. Consequently, Case 4 is the only possibility for ensuring $M_2 > 0$ and therefore (25), resulting in the following two conditions

$$\begin{aligned} C_2 + \alpha(C_5 + 1/2) &< 0 \quad (32) \\ k_{v_s} > \varphi_2(T, k_{p_s}, C_i, \alpha, M_m) &= \max\{\text{Root}(M_2)\} \quad (33) \end{aligned}$$

In the above discussion, to ensure $M_2 > 0$, a lower bound on k_{v_s} was imposed. Alternatively, an upper bound on T can be derived to fulfil $M_2 > 0$. To this end, note that $M_2 = m'_2 T + n'_2 > 0$ where, due to (32), $m'_2 = (m_2 k_{v_s}^2 + p_2)/T < 0$ and $n'_2 = n_2 k_{v_s} > 0$. Therefore, (33) and the following upper bound on T have the same effect

$$T < \zeta_2(k_{v_s}, k_{p_s}, C_i, \alpha, M_m) = -\frac{n'_2}{m'_2} \quad (34)$$

C. $j = 3$

We have

$$\Delta_3 = Q_3(M_3 + N_3/k_e + P_3/k_e^2) \quad (35)$$

where $Q_3 > 0$. Assuming $T^2, \dots, T^6 \approx 0$, we have

$$\begin{aligned} M_3 &= -M_m^2 T C_5 (1 + C_5) [C_2 + \alpha(1 + C_5)] \\ N_3 &= m_3 k_{v_s}^2 + n_3 k_{v_s} + p_3 \\ P_3 &= -T k_{p_s}^2 (M_m + \alpha M_s)^2 (C_2 + \alpha C_5) \end{aligned}$$

where

$$\begin{aligned} m_3 &= -T(C_2 + \alpha C_5)(M_m + \alpha M_s)[C_2 + \alpha(1 + C_5)] \\ n_3 &= 2M_m[C_2 + \alpha(1 + C_5)][-C_2 M_s + M_m(1 + C_5)] \\ p_3 &= a_3(M_m - \alpha M_s)^2 + b_3(M_m - \alpha M_s) + c_3 \quad (36) \end{aligned}$$

and a_3 and b_3 are functions of the system and control parameters and the sampling time, and

$$c_3 = -2T\alpha M_s^2 k_{p_s} [\alpha^2(1 + C_5) - 2C_2(C_2 + \alpha C_5)] \quad (37)$$

Due to (22) and (26), we have $M_3 > 0$. Therefore, if $P_3 < 0$, then $N_3^2 - 4M_3P_3 > 0$ implying that (35) will have a negative and a positive root with respect to k_e . As a result, if $P_3 < 0$, since $M_3 > 0$ the condition $\Delta_3 > 0$ will hold only if k_e is greater than the positive root, amounting to a nonzero, positive γ_1 in breach of (25). Therefore, we are only interested in $P_3 > 0$, which leads to (31).

Having ensured $P_3 > 0$, we distinguish the following two cases:

- Case 1: $N_3^2 - 4M_3P_3 < 0$. In this case, since $M_3 > 0$, the condition $\Delta_3 > 0$ will hold regardless of k_e .
- Case 2: $N_3^2 - 4M_3P_3 \geq 0$. In this case, we need $N_3 > 0$ in order to ensure (25). Otherwise, since $M_3 > 0$ and $P_3 > 0$, (35) will have two real positive roots, resulting in a nonzero, positive lower bound on k_e .

The expression $N_3^2 - 4M_3P_3$ can be viewed as a second-order polynomial in T or a fourth-order polynomial in k_{v_s} . In the following, we discuss why Case 1, i.e., $N_3^2 - 4M_3P_3 < 0$, is not an option regardless of how it is viewed:

- Implications of $N_3^2 - 4M_3P_3 < 0$ on T : It turns out that $N_3^2 - 4M_3P_3 = m_3'T^2 + n_3'T + p_3'$, where $p_3' = (n_3k_{v_s})^2 > 0$. We distinguish the following four cases:

- Case 1: $m_3' < 0$ and $n_3'^2 - 4m_3'p_3' < 0$. This is impossible because we know that $p_3' > 0$.
- Case 2: $m_3' < 0$ and $n_3'^2 - 4m_3'p_3' \geq 0$. In this case, since $p_3' > 0$, the second-order polynomial has one real positive and one real negative solution. In order to have $N_3^2 - 4M_3P_3 < 0$, the sampling period T needs to be greater than the positive root. However, a non-zero lower bound on T is not acceptable because as $T \rightarrow 0$, the discrete-time system approaches the continuous-time system, which was proven stable in Section III.
- Case 3: $m_3' > 0$ and $n_3'^2 - 4m_3'p_3' < 0$. In this case, $N_3^2 - 4M_3P_3 < 0$ never happens.
- Case 4: $m_3' > 0$ and $n_3'^2 - 4m_3'p_3' \geq 0$. In this case, again since $p_3' > 0$, depending on the sign of n_3' , the second-order polynomial has either two real negative or two real positive solutions, and $N_3^2 - 4M_3P_3 < 0$ holds if T is between the two solutions. For the negative solutions, this is impossible as $T > 0$ and for the positive solutions, it is unacceptable to put a non-zero lower bound on T .

- Implications of $N_3^2 - 4M_3P_3 < 0$ on k_{v_s} : The coefficient of $k_{v_s}^4$ in $N_3^2 - 4M_3P_3$ is equal to $m_3'' > 0$. The polynomial can either have four distinct real roots or two distinct real roots and two complex conjugate roots (note that if it has four complex conjugate roots, then $N_3^2 - 4M_3P_3 < 0$ will not hold as the coefficient of $k_{v_s}^4$ is positive; also, note that duplicate real roots do not change the sign of a polynomial). In order to have $N_3^2 - 4M_3P_3 < 0$, assuming roots $k_{v_{s1}} < k_{v_{s2}} < k_{v_{s3}} < k_{v_{s4}}$, we need either $k_{v_{s1}} < k_{v_s} < k_{v_{s2}}$ or $k_{v_{s3}} < k_{v_s} < k_{v_{s4}}$, in both cases imposing an upper bound on k_{v_s} . Consequently, this case is not of interest as such upper bounds on k_{v_s} should be avoided as far as possible.

In summary, $N_3^2 - 4M_3P_3 < 0$ imposes a lower bound on T and an upper bound on k_{v_s} . While for specific choices of T

and k_{v_s} such bounds may not create difficulties, in a general analysis they need to be avoided for the reasons explained earlier. Therefore, due to the unacceptable conditions that $N_3^2 - 4M_3P_3 < 0$ imposes on T and k_{v_s} , we only seek conditions that ensure Case 2, i.e., $N_3^2 - 4M_3P_3 \geq 0$ and $N_3 > 0$.

1) Conditions for ensuring $N_3 > 0$

The expression for N_3 is of second order in k_{v_s} , $N_3 = m_3k_{v_s}^2 + n_3k_{v_s} + p_3$, or of first order in T , $N_3 = m_3'T + n_3''$.

a) N_3 as a function of k_{v_s}

Noting that $m_3 > 0$ as a result of (26) and (31), we distinguish the following two cases.

- Case 1: $n_3^2 - 4m_3p_3 < 0$. In this case, $N_3 > 0$ holds for all values of k_{v_s} , thus no new condition is imposed.
- Case 2: $n_3^2 - 4m_3p_3 > 0$. A lower bound equal to the larger root of $N_3 = 0$ will be imposed on k_{v_s} .

In practice, the constant $\alpha = C_m/C_s$ is often chosen to be

$$\alpha = \frac{M_m}{M_s} \quad (38)$$

as the master and the slave control actions need to be proportional to their inertias. This will ensure that the master and the slave have similar closed-loop behavior. Choosing α according to (38) simplifies p_3 to c_3 and therefore, based on (21), (22) and (31), $p_3 < 0$. Also, with (38),

$$n_3^2 - 4m_3p_3 = -4\alpha^2 M_s^3 [C_2 + \alpha(1 + C_5)] R_3 \quad (39)$$

where

$$\begin{aligned} R_3 &= R_3' k_{p_s} T^2 - R_3'' \\ R_3' &= 4[\alpha^2(1 + C_5) - 2C_2(\alpha C_5 + C_2)](\alpha C_5 + C_2) \\ R_3'' &= M_s [C_2 + \alpha(1 + C_5)] [-C_2 + \alpha(1 + C_5)]^2 \end{aligned} \quad (40)$$

Due to (21), (22), (26) and (31), we have $R_3' < 0$ and $R_3'' > 0$. Therefore, $R_3 < 0$ regardless of T and based on (39), Case 1 never happens. Since $m_3 > 0$, in Case 2, the root of $N_3 = 0$ lower bounds k_{v_s} :

$$k_{v_s} > \varphi_4(T, k_{p_s}, C_i, \alpha, M_m, M_s) = \max\{\text{Root}(N_3)\} \quad (41)$$

Since $m_3 > 0$ and $p_3 < 0$, $N_3 = 0$ has a positive root and therefore in (41), $\varphi_4 > 0$.

b) N_3 as a function of T

If arranged as $N_3 = m_3''T + n_3'''$,

$$\begin{aligned} m_3'' &= m_3''' k_{v_s}^2 + n_3''' \\ n_3''' &= 2\alpha k_{v_s} M_s^2 [-C_2 + \alpha(1 + C_5)] [C_2 + \alpha(1 + C_5)] \end{aligned} \quad (42)$$

where

$$\begin{aligned} m_3''' &= -2\alpha M_s [C_2 + \alpha(1 + C_5)] (C_2 + \alpha C_5) \\ n_3''' &= -2\alpha k_{p_s} M_s^2 [\alpha^2(1 + C_5) - 2C_2(C_2 + \alpha C_5)] \end{aligned} \quad (43)$$

We need to have $n_3''' > 0$, resulting in

$$-C_2 + \alpha(1 + C_5) > 0 \quad (44)$$

Otherwise, either $N_3 > 0$ is impossible (if $m_3'' < 0$) or imposes a lower bound on T (if $m_3'' > 0$) which is not acceptable as was discussed earlier. Also note that $m_3''' > 0$

and $n_3''' < 0$ as a result of (21), (22), (26) and (31). Having ensured $n_3'' > 0$, we distinguish the following two cases.

- Case 1: $m_3'' < 0$. In this case, an upper bound on T (to satisfy $N_3 > 0$) and an upper bound on k_{v_s} (to satisfy $m_3'' < 0$) are simultaneously imposed.
- Case 2: $m_3'' > 0$. In this case, no condition on T (to satisfy $N_3 > 0$) and a lower bound on k_{v_s} (to satisfy $m_3'' > 0$) are imposed.

As was discussed earlier, we would like to avoid an upper bound on k_{v_s} as much as possible. Therefore, we opt for Case 2, which imposes the following condition on k_{v_2} :

$$k_{v_s} > \zeta_3(k_{p_s}, C_i, \alpha, M_s) = \sqrt{\frac{-n_3'''}{m_3''}} \quad (45)$$

2) Conditions for ensuring $N_3^2 - 4M_3P_3 \geq 0$

Since $N_3^2 - 4M_3P_3$ is a fourth-order polynomial in k_{v_s} in which the coefficient of $k_{v_s}^4$ is positive, the following condition is sufficient for $N_3^2 - 4M_3P_3 > 0$

$$k_{v_s} > \varphi_5(T, k_{p_s}, C_i, \alpha, M_m, M_s) \quad (46)$$

where

$$\varphi_5 = \max\{\text{Root}(N_3^2 - 4M_3P_3)\} \quad (47)$$

Again, $N_3^2 - 4M_3P_3$ can be viewed as a second-order polynomial in T leading to a similar constraint involving k_{v_s} and T , which is not discussed here for brevity.

D. $j = 4$

While conditions (20) for $j = 1, 2, 3$ imposed conditions on $C_2, C_5, \alpha, T, k_{p_s}$ and k_{v_s} such that the teleoperation system is stable with the slave in free space (i.e., $\gamma_1 = 0$ in (23)), condition $\Delta_4 > 0$ affects both the lower bound γ_1 and the upper bound γ_2 . Therefore, we split the discussion into the following two parts.

1) Slave in free space; $k_e = 0$

While we previously derived lower bounds on k_{v_s} , condition $\Delta_4 > 0$ also puts an upper bound on k_{v_s} . Indeed, excessively high values for k_{v_s} can cause $\Delta_4 < 0$ when $k_e = 0$, jeopardizing stability when the slave is in free space. To investigate this issue, assuming $T^3, \dots, T^{10} \approx 0$, we have

$$\Delta_4 |_{k_e=0} = Q_4(M_4k_{v_s}^2 + N_4k_{v_s} + P_4) \quad (48)$$

where $Q_4 > 0$ and

$$\begin{aligned} M_4 &= 256T^2k_{p_s}^2(M_m + \alpha M_s)^3(C_2 + \alpha C_5) \\ N_4 &= -512TM_mM_s k_{p_s}^2(M_m + \alpha M_s)^2(C_2 + \alpha C_5) \\ P_4 &= 256T^2M_mM_s k_{p_s}^3(M_m + \alpha M_s)^2(C_2 + \alpha C_5) \end{aligned}$$

Therefore, based on (31), $M_4 < 0$, $N_4 > 0$ and $P_4 < 0$. In order to have $\Delta_4 |_{k_e=0} > 0$, it is required that $N_4^2 - 4M_4P_4 > 0$, which results in the following condition:

$$k_{p_s}T^2 < \varphi_6(\alpha, M_m, M_s) = \frac{M_mM_s}{M_m + \alpha M_s} \quad (49)$$

When (49) holds, (48) has two positive roots, which are the lower and upper bounds on k_{v_s} such that $\Delta_4 |_{k_e=0} > 0$

$$\varphi_7 < k_{v_s} < \varphi_8 \quad (50)$$

where

$$\varphi_7 = \min\{\text{Root}(\Delta_4 |_{k_e=0})\} \quad (51)$$

$$\varphi_8 = \max\{\text{Root}(\Delta_4 |_{k_e=0})\} \quad (52)$$

2) Slave in contact with an environment; $k_e \neq 0$

Condition $\Delta_4 > 0$ decides the upper bound on k_e , i.e., γ_2 . While taking $i = 3$ or $i = 5$ in (18) yield similar results with respect to γ_1 , using $i = 5$ gives a less conservative (i.e., larger) γ_2 . However, increasing the order of approximation in (15) to $\mathcal{O}(T^8)$ affects γ_2 negligibly. With $i = 5$ in (18) and assuming $T^4, \dots, T^{10} \approx 0$, we have

$$\Delta_4 |_{k_e \neq 0} = R'_4(M'_4k_e^3 + N'_4k_e^2 + P'_4k_e + Q'_4) \quad (53)$$

where $R'_4 > 0$, and N'_4, P'_4 and Q'_4 are polynomials in k_{v_s} of orders 3, 4, and 2, respectively. Also,

$$M'_4 = \frac{256}{3}T^3M_m^3k_{v_s}C_5(1 + C_5)[C_2 + \alpha(1 + C_5)] \quad (54)$$

Based on (22) and (26), $M'_4 < 0$. This means that $k_e \rightarrow \infty$ causes $\Delta_4 < 0$ and thus the system becomes unstable. The upper bound on k_e is obtained as

$$\begin{aligned} k_e &\leq \gamma_2(T, k_{p_s}, k_{v_s}, C_i, \alpha, M_m, M_s) \\ &= \max\{\text{Root}(\Delta_4 |_{k_e \neq 0})\} \end{aligned} \quad (55)$$

Again, (53) can be viewed as a 3rd-order polynomial in T , which imposes an upper bound on T if k_e and k_{v_s} are given. Also, (53) is a 4th-order polynomial in k_{v_s} imposing lower and upper bounds on k_{v_s} for given T and k_e .

E. $j = 5, 6$

As was mentioned earlier, for $i = 3$ in (18), we will have terms up to Δ_4 in (20). For $i = 5$ in (18), there will also be Δ_5 and Δ_6 . However, in this case it can be shown that the previous conditions ensuring $\Delta_1, \dots, \Delta_4 > 0$ also ensure $\Delta_5 > 0$ and $\Delta_6 > 0$, thus no new additional conditions are imposed on the system and control parameters, the sampling time, or the environment stiffness.

VI. Simulation study

In order to further investigate the stability and performance of a teleoperation system under discrete-time control, we simulated a general 4-channel teleoperation system using SimuLink. In the simulation environment, Rate Transition blocks were used for realizing samplers and zero-order-holds in the block diagram of Figure 3. While the control blocks, which are shaded in Figure 3, were realized using z -domain transfer functions, the rest of the system was implemented using s -domain transfer functions. A variable-step, Dormand-Prince (ode45), continuous-time solver was used. The input \hat{f}_h simulates a human operator pushing the master at $t = 2 \rightarrow 7$ sec such that the slave makes contact with the environment, and retracting the master to the original position at $t = 7 \rightarrow 12$ sec. We chose $M_m = M_s = 1$ kg, $C_s = 20s + 100$, $\alpha = M_m/M_s = 1$, $C_2 = 0.2$, $C_5 = -0.75$, and based on (9), $C_6 = C_2 - 1 = -0.8$ and $C_3 = C_5 + 1 = 0.25$. These choices meet the design conditions derived in Section V for ensuring stability.

Figure 4 shows the maximum environment stiffness for a given sampling time such that teleoperation remains stable for the cases of $i = 3$ (i.e., V_3), $i = 5$ (i.e., V_5), and simulations. As expected and similar to the case of a discretely-simulated virtual wall with stability condition (2), higher sampling periods allow for lower maximum environment stiffnesses (k_e can vary from zero up to γ_2). As can be seen, increasing i in (18) from 3 to 5 enhances the precision of the upper bound on k_e given by (55). It was confirmed by both analysis and simulation that further increase in i to 7 or

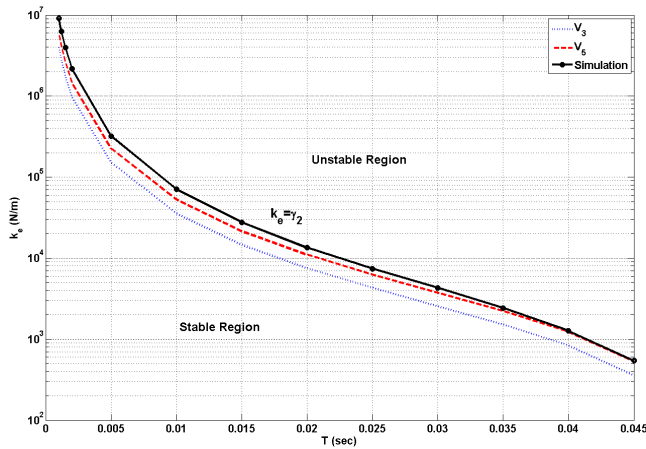


Fig. 4. Stability/instability regions in k_e - T plane for $k_{v_s} = 20$.

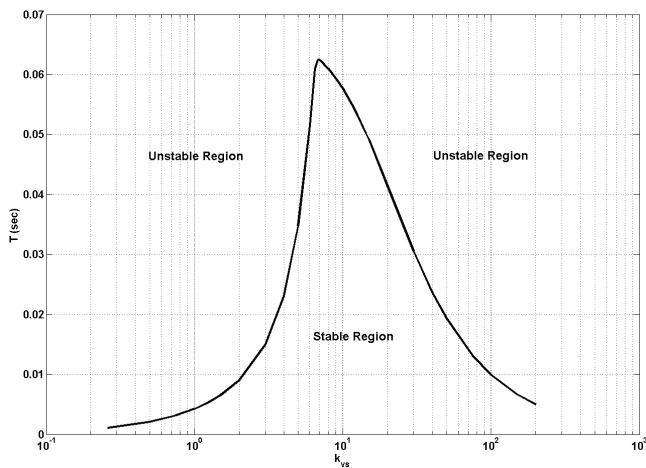


Fig. 5. Stability/instability regions in T - k_{v_s} plane for $k_e = 1000$ N/m.

9 has a negligible effect on the precision of γ_2 (the obtained curves coincide with that of $i = 5$).

When $i = 5$, the order of precision of the differentiation method affects the accuracy of γ_2 as given by (55). For instance, it was observed that using $s = T/(z - 1)$ or $s = Tz/(z - 1)$ (based on backward- and forward-rectangular integration) instead of $s = 2(z - 1)/(T(z + 1))$ (based on Trapezoidal integration) in determining (17) drives γ_2 very distant from the simulation results. In fact, increasing the order of precision of differentiation reduces the distance between the theoretical and the simulation results at the cost of higher computational complexity and less mathematical tractability.

Figure 5 illustrates the effect of the damping introduced by the controller on the maximum allowable sampling period for a typical environment stiffness $k_e = 1000$ N/m (the same simulation parameters as before were used). From (50), the stabilizing range of k_{v_s} for $k_e = 0$ is $0 < k_{v_s} < 200$. As can be seen in Figure 5, added damping up to $k_{v_s} = 6.8$ has a constructive effect on system robust stability while further increase in damping reduces the maximum allowable sampling period. Simulation results precisely match the theoretical results of Figure 5 for $T \leq 49$ msec and therefore they are not shown separately. For $T > 49$ msec, the fact that high orders of T were ignored during the stability analysis for less complexity causes some discrepancy between the simulation results and the outcome of the theoretical analysis.

VII. Conclusions

In this paper, first the hybrid model of the digitally controlled 4-channel teleoperation system was derived. Next, without making any assumption about the human operator dynamics, regions of stability of the discrete-time controlled teleoperation system were obtained in the form of conditions on the control parameters, sampling period and environment stiffness. Specifically, requirements on the control parameters and the sampling period were found such that stability is ensured when the slave is in free space. It was shown that when the slave is in contact with an environment, stability conditions involve upper bounds on the sampling period. These theoretical results were confirmed by a simulation study in which the bilateral controller was realized by z -domain transfer functions while the master, the slave and the environment were simulated in the s -domain. Since in real life the human operator has an impedance with a finite dynamic range and acts as a negative and stabilizing feedback, the stability regions found in this paper correspond to a worst-case scenario due to their independence from the operator's dynamical characteristics.

References

- [1] R. Gillespie and M. Cutkosky, "Stable user-specific rendering of the virtual wall," in *Proceedings of the ASME International Mechanical Engineering Conference and Exposition*, vol. 58, Atlanta, GA, November 1996, pp. 397–406.
- [2] R. Anderson, "Building a modular robot control system using passivity and scattering theory," in *Proceedings of IEEE International Conference on Robotics and Automation*, vol. 1, Minneapolis, MN, April 1996, pp. 698–705.
- [3] S. Stramigioli, C. Secchi, A. van der Schaft, and C. Fantuzzi, "A novel theory for sample data system passivity," in *Proceedings of the IEEE/RSJ International Conference on Intelligent Robots and Systems*, Lausanne, Switzerland, 2002, pp. 1936–1941.
- [4] G. Leung and B. Francis, "Bilateral control of teleoperators with time delay through a digital communication channel," in *Proceedings of the Thirtieth Annual Allerton Conference on Communication, Control and Computing*, 1992, pp. 692–701.
- [5] J. Colgate and G. Schenkel, "Passivity of a class of sampled-data systems: Application to haptic interfaces," *Journal of Robotic Systems*, vol. 14, no. 1, pp. 37–47, 1997.
- [6] J. Abbott and A. Okamura, "Effects of position quantization and sampling rate on virtual wall passivity," *IEEE Transactions on Robotics*, vol. 21, no. 5, pp. 952–964, October 2005.
- [7] J. Gil, A. Avello, A. Rubio, and J. Florez, "Stability analysis of a 1 dof haptic interface using the routh-hurwitz criterion," *IEEE Transactions on Control Systems Technology*, vol. 12, no. 4, pp. 583–588, July 2004.
- [8] L. Love and W. Book, "Contact stability analysis of virtual walls," in *Proceedings of the ASME International Mechanical Engineering Conference and Exposition*, vol. 57, no. 2, 1995, pp. 689–694.
- [9] D. A. Lawrence, "Stability and transparency in bilateral teleoperation," *IEEE Transactions on Robotics & Automation*, vol. 9, pp. 624–637, October 1993.
- [10] K. Hashtrudi-Zaad and S. E. Salcudean, "Analysis of control architectures for teleoperation systems with impedance/admittance master and slave manipulators," *The International Journal of Robotics Research*, vol. 20, no. 6, pp. 419–445, 2001.
- [11] N. Diolaiti, G. Niemeyer, F. Barbagli, and J. J.K. Salisbury, "Stability of haptic rendering: Discretization, quantization, time delay, and coulomb effects," *IEEE Transactions on Robotics*, vol. 22, no. 2, pp. 256–268, April 2006.
- [12] J. Gil, E. Sanchez, T. Hulin, C. Preusche, and G. Hirzinger, "Stability boundary for haptic rendering: Influence of damping and delay," in *IEEE International Conference on Robotics and Automation*, Rome, Italy, 2007, pp. 124–129.
- [13] L. Ni and D. W. L. Wang, "A gain-switching control scheme for position-error-based bilateral teleoperation: Contact stability analysis and controller design," *International Journal of Robotics Research*, vol. 23, no. 3, pp. 255–274, March 2004.